RESEARCH ARTICLE

VOLCANICA

Distinguishing shallow from mid-crustal magmatic processes at Soufrière Hills Volcano using Finite Element Modelling and co-analysis of EDM and GPS data

Alexander Johnson[α], James Hickey*[α], Karen Pascal[β,γ], Ben. J. Williamson[α], and Racquel Syers[β]

[α] Department of Earth and Environmental Sciences, University of Exeter, Cornwall, TR10 9FE, United Kingdom.
[β] Montserrat Volcano Observatory, Montserrat.
[γ] Seismic Research Centre, University of the West Indies, St. Augustine, Trinidad and Tobago.

Abstract

We modelled ground deformation at Soufrière Hills Volcano (SHV), using data collected by the Montserrat Volcano Observatory from 2010–2019. We investigate the combined use of Electronic Distance Measuring (EDM) and Global Positioning System (GPS) to distinguish shallow from mid-crustal magmatic processes and their surface deformation profiles. Our results suggest that the EDM network responds predominantly to changes in the shallow magmatic system, whereas GPS records variation at mid-crustal levels. In addition, we show that the behaviour of the EDM network, and of the GPS site HERM, can be explained by under-pressurisation in a shallow dyke conduit orientated NNW–SSE, while the mid-crustal system was still undergoing pressurisation. The modelled dyke may be responding to magma cooling and contraction associated with a previous intrusion. We find that geodetic monitoring coverage of multiple flanks within 1 km of the vent can improve our understanding of shallow magmatic system processes with asymmetric deformation fields.

Keywords: Electronic distance measurement; Global Position System; Ground deformation; Montserrat; Soufriere; Monitoring.

Submitted: 2022-03-28 | Accepted: 2023-07-19 | Published: 2023-08-17

Editor: S. K. Ebmeier | Typesetter: J. Farquharson

1 Introduction

Volcano deformation records the inflation or deflation of a volcanic edifice primarily caused by the movement of magma beneath the surface. Deformation signals are monitored using a variety of methods, including Electronic Distance Measurement (EDM), Global Position System (GPS), Interferometric Synthetic Aperture Radar (InSAR), tiltmeters, and strainmeters [Odbert et al. 2014; Spaans and Hooper 2016; Johnson et al. 2019]. Changes in deformation signals may indicate volcanic unrest, and when used in combination with other monitoring methods provide essential insight into the status of active volcanoes [Phillipson et al. 2013; Gottsmann et al. 2017]. Deformation can be caused by both magmatic processes, such as magma movement into a then-overpressurised magma reservoir [Geirsson et al. 2012], sheet intrusion [Biggs and Pritchard 2017], non-magmatic mechanisms such as movement of hydrothermal fluids [Fournier and Chardot 2012], the loading of deposits on the volcanic edifice [Odbert et al. 2015], flank collapse/instability [Bonaccorso et al. 2013], or the cooling of magma beneath the surface [Parker et al. 2014]. The intricacies of how magmatic processes produce surface deformation can be examined via the use of models, which require assumptions and simplifications to be made about magma behaviour and crustal mechanics, but can be a useful tool in understanding subsurface processes [Ranalli 1995; Masterlark 2007; Del Negro et al. 2009].

Analytical modelling, which has been used since the publication of the Mogi model [Mogi 1958], still provides a rapid and simple approach to modelling volcanic deformation. Analytical models require a significant set of assumptions to work; the crustal rheology is usually defined as an isotropic, homogeneous, elastic half space with a flat, free surface. Later analytical models have incorporated simple viscoelastic rheologies [Dragoni and Magnanensi 1989; Del Negro et al. 2009] or source shape variation [Yang et al. 1988; Fialko et al. 2001].

Numerical modelling, such as Finite Element Modelling (FEM), eliminates some of the disadvantages of analytical models by removing or relaxing some of their assumptions. Justification for additional model complexity, where observations can also support it, is afforded through increased understanding of rock mechanics, alongside geophysical, petrological, and geological evidence [e.g. Currenti et al. 2007; Masterlark 2007; Gottsmann and Odbert 2014; Hickey et al. 2017; Head et al. 2019; Taylor et al. 2021]. FEM allows for the introduction of realistic 3D topography [Hautmann et al. 2009; Hickey et al. 2020], anisotropic continuous mechanical heterogeneity [Currenti et al. 2007; Cabaniss et al. 2020; Gottsmann et al. 2020], and viscoelasticity if appropriate [Del Negro et al. 2009; Head et al. 2019; Sigmundsson et al. 2020].

Soufrière Hills Volcano (SHV) is an andesitic volcano located on the Caribbean island of Montserrat, part of the Lesser Antilles island arc (Figure 1). The SHV is currently in an intra-eruptive pause of an anomalously lengthy eruptive episode, which has been ongoing since 1995 [Christopher et al. 2014; Odbert et al. 2014; Wadge et al. 2014; Hickey et al. 2022]. Activity is typically characterised by phases of eruption comprised of lava dome growth and collapse, associated pyroclastic flows, and Vulcanian and sub-Plinian explosions [Sparks and Young 2002]. The volcano is monitored by a comprehensive network of GPS sites and EDM baselines (Figure 1)

* j.hickey@exeter.ac.uk

as well as strainmeters, occasional gravity monitoring, and—prior to their destruction in 1997—tiltmeters. During eruptions, ground deformation is characterised by deflation of the volcanic edifice, with associated subsidence and negative radial deformation (horizontal movement towards the vent) [Odbert et al. 2014; Neuberg et al. 2022]. Intra-eruptive pauses are often associated with steady inflation of the edifice, and positive radial deformation (horizontal movement away from the vent) [Hickey et al. 2022]. The current intra-eruptive repose period, from 2010 to present, is recorded by ongoing surface deformation inferred to be caused by pressurisation in a mid-crustal magma storage region [Hickey et al. 2022].

The mid-crustal SHV magmatic system has commonly been modelled as two vertically stacked and linked magma chambers connected to the surface by a dyke conduit complex [e.g. Elsworth et al. 2008; Hautmann et al. 2009; Linde et al. 2010; Mattioli et al. 2010; Gottsmann and Odbert 2014; Young and Gottsmann 2015]. However, some studies have shown that the stacked two-chamber system is indistinguishable from a single, large, prolate-shaped reservoir [Mattioli et al. 2010; Voight et al. 2010], and the most recent modelling studies into the SHV utilise the single prolate-shaped magma system model [Christopher et al. 2014; Gottsmann and Odbert 2014; Gottsmann et al. 2020; Hickey et al. 2022], which acts as a simplified reflection of the trans-crustal magmatic system as a whole [Christopher et al. 2014; Sparks and Cashman 2017].

Studies into the shallow system of the SHV have modelled the magmatic plumbing as a dyke conduit, extending from approximately 1 km below the vent [Widiwijayanti 2005; Costa et al. 2007; Voight et al. 2010; Odbert et al. 2014] to a magma source at around 6 km depth [Mattioli et al. 1998; Voight et al. 2006; Costa et al. 2007; Hautmann et al. 2009; Linde et al. 2010; Odbert et al. 2014]. These studies used a combination of GPS and strainmeter data to examine the shallow system, while EDM has so far not been used. A strain data–led study into a Vulcanian explosion in March 2004 examined the conduit by combining a Mogi source and Okada-style dyke model [Linde et al. 2010]. The results correspond with previous GPS-based models of a roughly northwest–southeast orientated dyke conduit [Mattioli et al. 1998; Hautmann et al. 2009], and thereby help to support the overall picture built up of the shallower dyke conduit part of the system. A further study examined volumetric strain data from the July 2008 Vulcanian explosion using a heterogeneous elastic finite element model [Young and Gottsmann 2015], and found the dyke conduit had a radius of ~40 m, and extended to a depth of ~1500 m from the vent. A narrower conduit with a radius of 15–25 m inferred from magma spine dimensions [Melnik and Sparks 2002; Loughlin et al. 2006] then connects the dyke conduit to the surface [Wadge et al. 2006].

A historical stumbling block for GPS-led modelling studies on the SHV has been the continuous GPS site HERM, situated on the north-eastern flank, and closer to the vent than any other GPS site currently in the monitoring network (Figure 1). The horizontal deformation recorded at this site is often anomalous when compared to the horizontal deformation patterns of the rest of the GPS network [Odbert et al. 2014] which has led to it being excluded from some GPS-led modelling studies [Mattioli et al. 2010; Gottsmann et al. 2020]. During the earlier stages of the eruptive episode at SHV, HERM continuously displayed high magnitude deformation to the northeast compared to the rest of the GPS network during both the eruptions and the intra-eruptive pauses following its installation in July 1996, with spikes in north-eastward movement occurring towards the end of eruptions in March 2001, June 2002, and July 2003 and immediately before eruptions in August 2005 and October 2009 [Odbert et al. 2014; Wadge et al. 2014]. The behaviour of HERM has previously been hypothesised as the emplacement of a secondary non-feeder dyke on the northeast side of the edifice between HERM and the vent, creating a decoupled wedge of land between two valleys on the basis of short term deformation patterns from data collected between 1998–2010 [McPherson 2013; Odbert et al. 2014]. Here we aim to reconcile two outstanding issues from previous modelling work at SHV; the anomalous deformation of GPS site HERM, and the lack of incorporation of EDM data in modelling. Specifically, we test how the shallow and deep portions of the magmatic system may produce different surface deformation footprints that are preferentially recorded by either the GPS or EDM network. We investigate whether there are additional modelling benefits to utilising the EDM sites, as they are located closer to the vent than the GPS network. Using the additional context of the EDM data in modelling the magmatic system, we present an alternative potential explanation for the behaviour of HERM and a discussion of the insights this GPS site, and the EDM network, can offer into the post-2010 behaviour of the magmatic system at SHV. We do not set out to accurately constrain an optimised model setup against the observed geodetic data.

2 Methods and data

2.1 GPS and EDM data

We used GPS- (Figure 2) and EDM- (Figure 3, Supplementary Material Figure S1) derived surface displacements from February 2010–September 2018 (GPS) and December 2019 (EDM), collected and processed by the Montserrat Volcano Observatory (MVO). The geodetic network at SHV has been steadily developed since the eruptive episode began in 1995, and now includes a comprehensive GPS network comprising 8 campaign and 14 continuous GPS sites as well as a set of up to 6 EDM baselines, some of them first established in the initial stages of the eruptive episode (Figure 1) [Jackson et al. 1998]. Daily positions and velocities of the GPS sites are calculated with the `GAMIT/GLOBK` GPS software (version 10.7), which uses the double-differencing processing methodology [Herring et al. 2018]. All displacements related to equipment changes are corrected for, the regional tectonic component is removed by calculating the GPS positions relative to the `ITRF2014` Caribbean plate motion model [**Altimini_2017**], and the GPS solutions are stabilised using a set of globally distributed reference stations with well-known positions. Differences between the GPS velocities presented here for 2010–2018 (Figure 2) and those of Neuberg et al. [2022] from 2012–2015 arise because of differences in the time period being analysed. During the current extended intra-eruptive pause, the GPS network as a

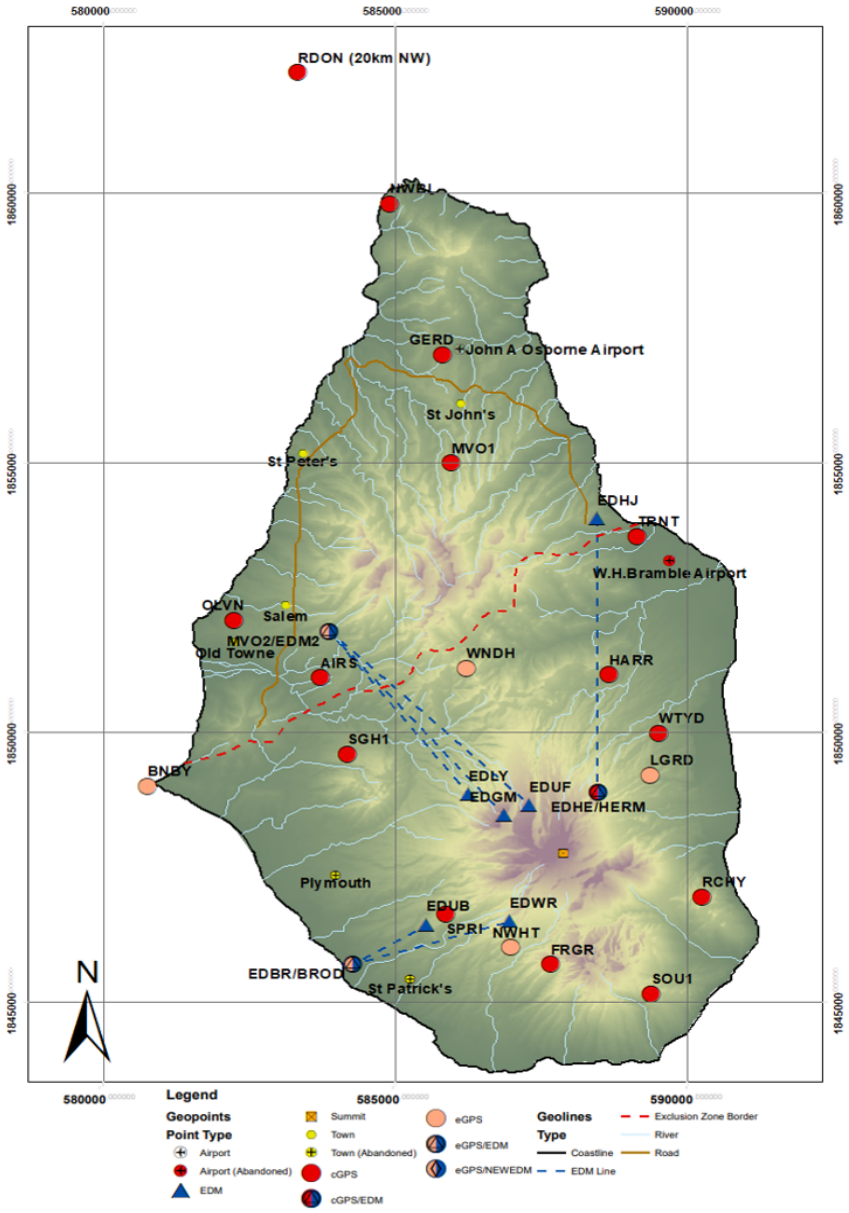

Figure 1: Map of MVO GPS and EDM monitoring network for 2010–2018. There is currently no EDM coverage of the south-eastern flank. The location of the vent has migrated over time, and the location marked is an approximation of the time-averaged position after Odbert et al. [2014]. cGPS = Continuous GPS sites, eGPS = Campaign GPS sites. DRYG is an eGPS site, which we have modelled as a prospective new EDM base station later in this paper.

whole has recorded steady vertical inflation of the edifice and horizontal displacements mostly directed away from the vent. However, the GPS site HERM deformed to the east-southeast, with positive vertical deformation (Figure 2).

The raw EDM data (Supplementary Material Figure S1) were inherently noisy, and showed large step-changes in line length associated with significant discrete volcanotectonic (VT) events that occurred in March 2012 (which involved ash venting and the creation of two small craters), and March 2014. To isolate and remove the effect of the VT events and reduce the influence of noise, the raw EDM data were corrected by assuming zero line length change over the VT event, which was implemented by calculating and subtracting the line length change produced by each VT event (Figure 3).

2.2 Model setup

Finite Element Modelling (FEM) with `COMSOL Multiphysics v5.5` was used to simulate the magmatic system at SHV; voids in the model space were used as proxies for magma bodies by pressurising their exterior surfaces (Figure 4). A full 3D model geometry was developed, implementing a 2014 Digital Elevation Model (DEM) of the island [Stinton 2015]. The inclusion of topography in our model is essential in order to accurately reflect the true three-dimensional geometry of the EDM lines used in this study, i.e. their line-of-sight from the base of the edifice to a point on the edifice. We used prolate cavities, and in the case of the shallow dyke a rectangular cuboid cavity, to simulate deformation sources. To represent the mid-crustal

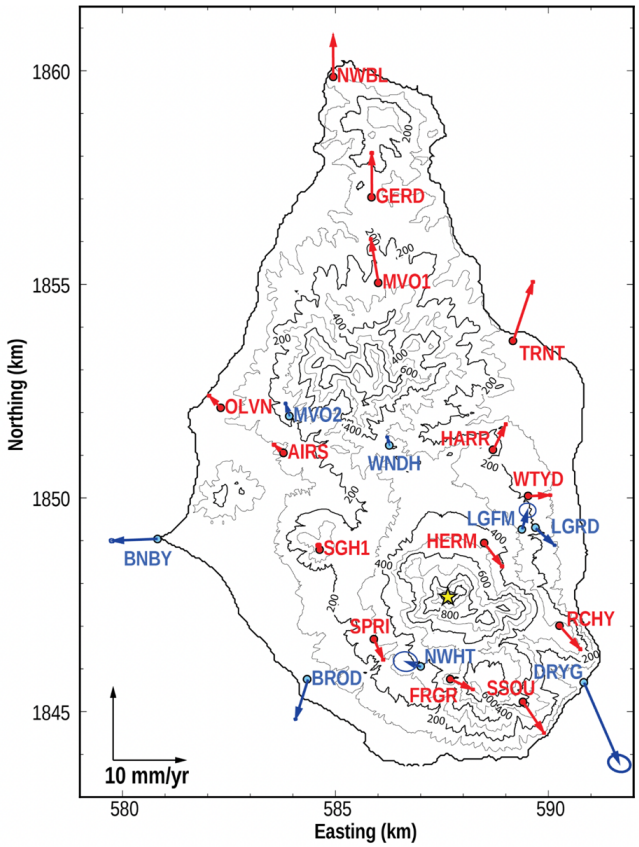

Figure 2: 2010–2018 horizontal GPS velocities. Horizontal GPS velocities vectors observed by MVO from 2010–2018, calculated relative to the Caribbean tectonic plate velocity model. The vent is marked with a yellow star, Continuous and Campaign GPS sites names and velocities are indicated in red and blue, respectfully. The length of the arrow is an indicator of the scale of deformation, and the size of the error ellipse represents the 95 % error.

magmatic system, we used a single large prolate source with an x-axis of 2000 m, y-axis of 2000 m, z-axis of 4000 m, and centred at a depth of 9500 m [Gottsmann et al. 2020]. The model domain was large enough to avoid boundary effects (60 × 60 × 30 km), and an infinite element domain also surrounded the model geometry to further aid this. A tetrahedral mesh was used with higher mesh density surrounding the sources and volcanic edifice. A roller boundary surrounds the model, and the base of the model is fixed [Hickey and Gottsmann 2014]. Heterogeneous elastic behaviour was assumed for the rheology, with 3D variations in density and (dynamic) Young's modulus constrained using a 3D seismic P-wave velocity model [Paulatto et al. 2012; Hickey et al. 2022], alongside a constant Poisson's Ratio of 0.25. We use an elastic rheology to focus our efforts on the spatial deformation pattern rather than time-dependent phenomena. The position change of GPS and EDM points derived from the monitoring network and placed into the model geometry were recorded. For EDM lines the relative changes of each end of a baseline were used to calculate the modelled line length variation.

2.3 Modelling approach

We utilise the prolate source model proposed by Gottsmann et al. [2020] as a proxy for the mid-crustal magmatic system (Figure 4, Table 1). All model simulations include an active mid-crustal deformation source to reflect recorded pressurisation in the magmatic system beneath the volcano during our time period of interest [Hickey et al. 2022]. Using a series of forward models, we experimented with the further addition of a shallow prolate source or dyke in order to explore differences in how the island's EDM and GPS monitoring networks record changes to pressurisation in different parts of the magmatic system. To do this we investigated three main scenarios. In step one (Figure 4B), we modelled the mid-crustal reservoir in isolation and conducted sensitivity tests on each source parameter independently (Table 1) to observe the mid-crustal magmatic system's effect on the surface deformation footprint. Sensitivity tests were conducted by independently varying a single parameter through a range of values (while all other parameters remained constant at a default value) and measuring the effect on surface deformation. This was undertaken in two stages: in step 1a, a wide set of parameter values were examined and the optimal value used to define the starting point for step 1b, which had a narrower set of parameter values and smaller step changes (Table 1). The initial source parameters for step 1a were based on model results derived from analysis of GPS data from 2003 [Gottsmann et al. 2020], so we also compared our modelled results to the recorded 2010–2018/19 GPS and EDM data to derive a slightly modified preferred set of mid-crustal source parameters for this more recent deformation period. The updated mid-crustal reservoir parameters were also used in steps two and three.

In step two (Figure 4C), we added a second, smaller, shallow, prolate reservoir between the top of the mid-crustal magmatic system and the edifice. The mid-crustal magmatic system was kept fixed (using the updated solutions from step 1b), and sensitivity tests were conducted on the parameters defining the shallow source (Table 2). The shallow prolate source parameters were based on previous results examining this part of the magmatic system [Mattioli et al. 1998; Voight et al. 2006; Wadge et al. 2006; Elsworth et al. 2008; Hautmann et al. 2013]. Finally, in step three (Figure 4D), we replaced the shallow prolate source with a dyke conduit and conducted further sensitivity tests (Table 3). To simulate the shallow magmatic system as a dyke conduit, a single rectangular cuboid source 500 m wide and 50 m thick was used [Mattioli et al. 1998; Costa et al. 2007; Hautmann et al. 2009; Linde et al. 2010] and extended from approximately 200 m below sea level (1.2 km below the vent) to a depth of 5.2 km below sea level. However, we used a thicker dyke (50 m) compared to previous estimates (2 m) to reduce the computational cost of our approach; a 2 m thick dyke in a 60 km wide model geometry required a computational mesh that was too dense for the efficient building and solving of the numerical model with available computer power and time. To confirm our modification would not produce erroneous results, we computed a simple comparison of a 2 m- and a 50 m-wide dyke using a 2D Finite Element model, and found that the increase in dyke thickness when applying the same uniform pressure increase

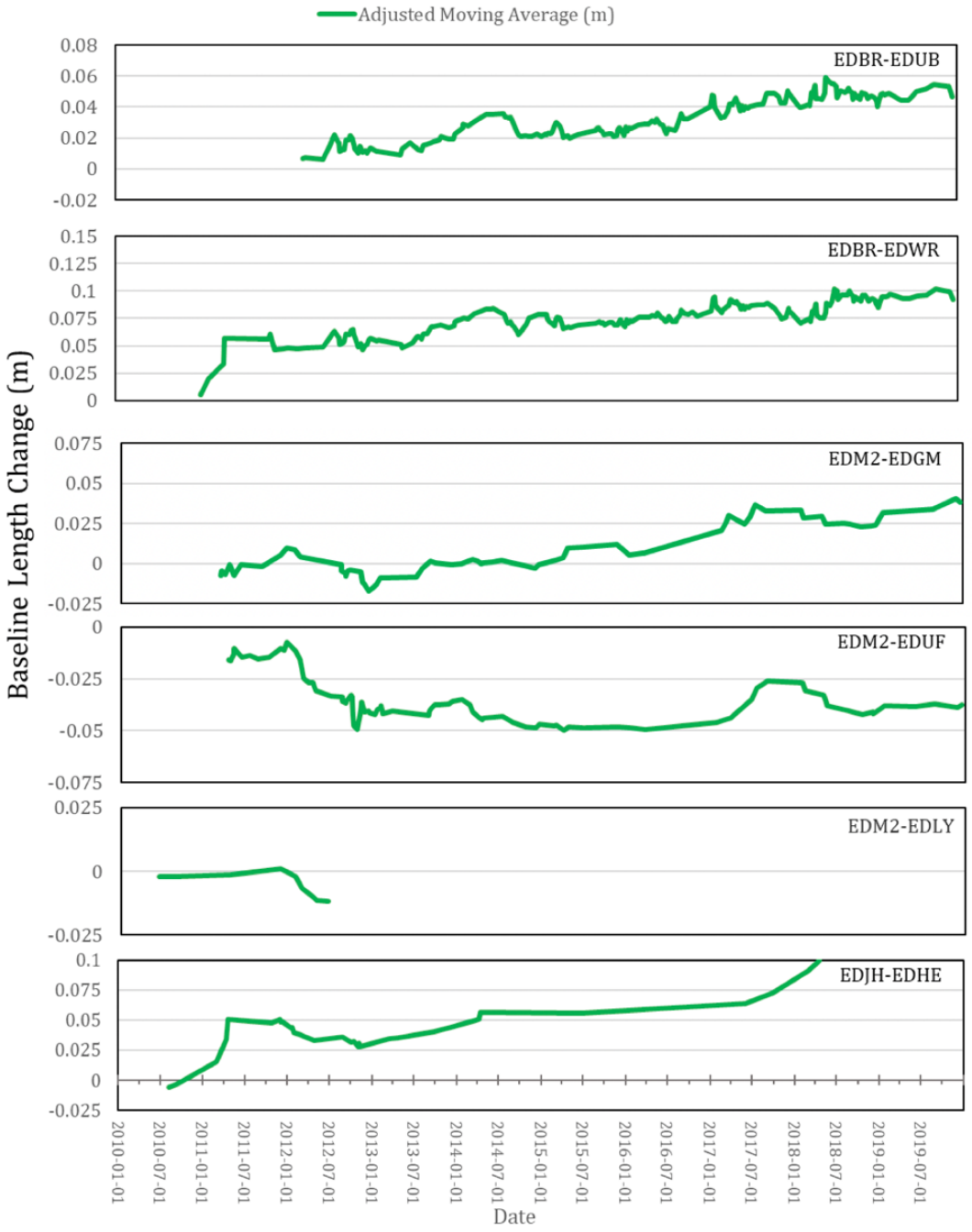

Figure 3: Observed EDM baseline length changes between 2010 and 2019, adjusted for significant volcanotectonic (VT) events in March 2012 and March 2014. Individual EDM data points are shown in Supplementary Figure 1.

made no significant difference to the surface deformation response (Supplementary Material Figure S2). Within step 3, a preliminary sensitivity test (step 3a) was undertaken for all parameters, which found that pressure and orientation were the two most important factors. The preliminary sensitivity tests also found that a better fit to the observed data was achieved with a shallower dyke depth, so for subsequent models in step 3b the dyke conduit extended from 0.5 km above sea level to 4.5 km below sea level, approximately 500 m shallower than in previous studies. From the results of the preliminary sensitivity tests (step 3a) we found pressure and orientation to be the two most significant parameters. We therefore ran a co-parametric sensitivity test (step 3b) of pressure and orientation simultaneously with the updated dyke geometry, including with negative overpressures (Table 3). Conditions for the mid-crustal magmatic system were kept constant at 10 MPa with no change in strike or tilt of the prolate source for both shallow source experiments (steps two and three), and results were again compared to the recorded 2010–2018/19 EDM and GPS data.

We compare our model results to the GPS and EDM datasets using a misfit function adapted from Hickey [2015]

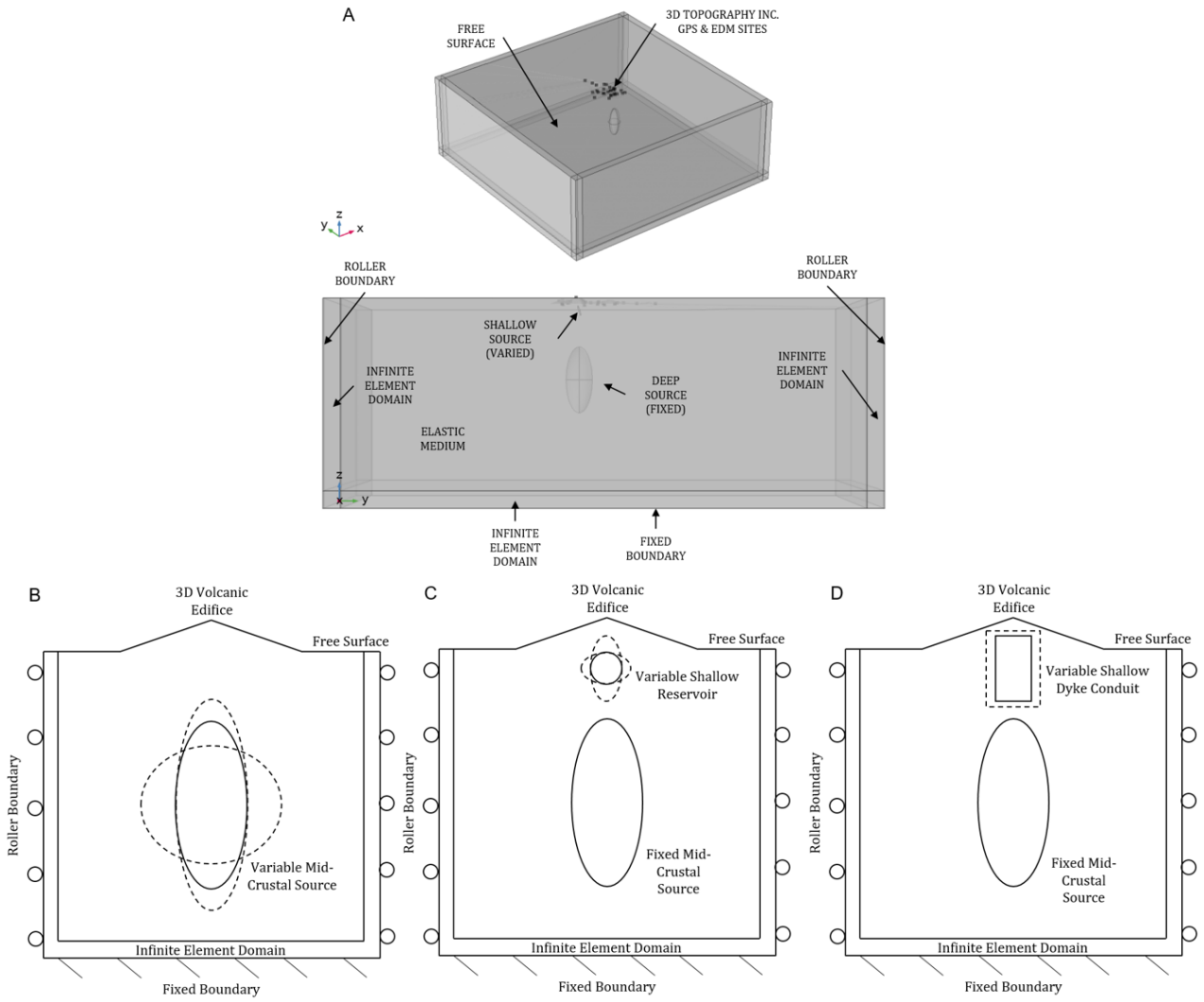

Figure 4: Schematic diagrams of 3D Finite Element Model setup. The model is 3D in order to include the 3D topography of the island and non-axisymmetric deformation sources. The model size is 60 × 60 × 30 km, and an infinite element domain incorporated, to prevent boundary conditions from interfering with interior results. The mesh was refined on the magma bodies and island topography. The domain is elastic. The base of the model is a fixed boundary, with roller boundaries on the edges and a free surface on top. [A] 3D view of the model geometry with 3D topography. [B] Sketch of model geometry for variation of mid-crustal reservoir (Table 1). [C] Sketch of model geometry for variation of a shallow reservoir (Table 2). [D] Sketch of model geometry for variation of a shallow dyke conduit (Table 3).

to numerically evaluate how changes to the magmatic system affect the overall fit to the geodetic data. The misfit function, J, is defined as:

$$J = \sqrt{\sum f_i} \tag{1}$$

$$f_i = [(M_i - D_i) \times W_i]^2 \tag{2}$$

$$W_i = \frac{a_i}{\sum a_i} \tag{3}$$

$$a_i = \left| \frac{D_i}{E_i} \right| \tag{4}$$

where M corresponds to the modelled deformation, D corresponds to the observed deformation, E corresponds to the error, W corresponds to the weighting, and i is the index for each individual EDM baseline or GPS vector. The misfit function value was calculated for both GPS and EDM for each model iteration. The lower the misfit function value, the better the fit of the model to the observed data, and the greater the variation in the misfit function values for a given sensitivity test, the greater role that source parameter plays in dictating the surface deformation response. A full inversion of the data was beyond the scope of our study.

Following the findings of the dyke conduit study, we further experimented with two new prospective EDM lines by adding a new EDM reflector (ENEW1) site on the south-eastern flank relatively close to the vent with an EDM baseline extending down to the pre-existing GPS site DRYG (DRYG–ENEW1), and a new EDM base station (ENEW2) on the southern coastline with a baseline extending up to the pre-existing reflec-

Table 1: 3D source parameters used in modelling the mid-crustal reservoir. The reservoir was modelled in two stages, the first being a wide range of values, and the second a more refined range based on the findings of the first. The parameter values for both ranges are provided below. Default values are from Gottsmann et al. [2020].

Source parameters (Mid-crustal reservoir)					
Parameter	Stage	Low margin	Default	High margin	
Depth (midpoint) (m)		8000	9500	15 000	250
X-location		583 500	588 500	593 500	1000
Y-location		1 843 280	1 848 280	1 853 280	1000
a (x)-axis (m)	1A	1400	1890	2400	50
b (y)-axis (m)	1A	1500	2010	2500	50
c (z)-axis (m)	1A	4500	5010	5500	50
a (x)-axis (m)	1B	1840	1890	1940	5
b (y)-axis (m)	1B	1960	2010	2060	5
c (z)-axis (m)	1B	4960	5010	5060	5
Source strike (°)	1A	0	0	330	30
Source strike (°)	1B	−6.2	−1.2	3.8	1
Source dip (°)	1A	−125	10	125	25
Source dip (°)	1B	0	9	14	1
Source heading (°)	1A	0	0	360	15
Source heading (°)	1B	118	128	138	5
Pressure (MPa)		1	11	21	1

Table 2: 3D source parameter table used in the modelling of a shallow reservoir. Mid-crustal source parameters are from the results of step 1 (described in the text).

Source Parameters (Shallow Reservoir)					
Parameter	Mid-crustal source	Shallow source			Step
		Low margin	Default	High margin	
Depth (m)	9500	500	1500	2500	100
X-location	588 500	583 500	588 500	593 500	1000
Y-location	1 848 280	1 843 280	1 848 280	1 853 280	1000
a (x)-axis (m)	2000	100	500	1000	100
b (y)-axis (m)	2000	100	500	1000	100
c (z)-axis (m)	4000	100	500	1000	100
Source strike (°)	0	0	180	330	30
Source dip (°)	0	0	180	330	30
Source heading (°)	0	0	180	330	30
Pressure (MPa)	10	−25	20	25	1

tor EDWR (ENEW2–EDWR). These sites were chosen to explore the deformation response on a part of the island with no present EDM coverage, and to see if the pattern of EDM line behaviour seen on the north and west of the vent is mirrored.

3 Results and Discussion

3.1 Mid-crustal magmatic system

Varying the parameters of a single, large, prolate source could not explain the pattern of observed EDM deformation alone (Figure 5), consistently either overestimating line length change on EDM2–EDLY/EDUF/EDGM on the north-western flank, or underestimating line length change on EDJH–EDHE (north-eastern flank), and to a lesser extent, underestimating line length change on EDBR–EDWR/EDUB (south-western flank). This pattern was repeated for all parameters tested, with the mid-crustal source producing a symmetrical deformation field which could not account for the asymmetric EDM line length changes observed. The GPS response to mid-crustal source parameter variation is broadly in line with observed data, with sites placed far from the vent experiencing more horizontal deformation than sites close to the vent. Notably, this model also could not account for the observed movement of HERM.

Naturally, the misfit function results for the GPS network provided a closer fit to the observed values than the EDM network (Figure 6), as the mid-crustal magmatic system geometry was optimised on GPS data from 2003 [Gottsmann et al. 2020]. Varying the depth of the source also showed that EDM is unresponsive to changes in a mid-crustal source when compared

Table 3: 3D source parameter tables used in modelling the variation in a dyke conduit source. [A] Preliminary sensitivity test parameters (step 3a); [B] Co-parameter variation (step 3b).

[A] Source parameters (dyke conduit sensitivity tests)					
Parameter	Mid-crustal source	Dyke conduit (Rectangular Cuboid)			Step
		Low margin	Default	High margin	
Depth (midpoint) (m)	9500	2500	3500	5000	100
X-location	588 500	583 500	588 500	593 500	1000
Y-location	1 848 280	1 843 280	1 848 280	1 853 280	1000
a (x)-axis (m)	2000	100	500	1100	100
b (y)-axis (m)	2000	N/A	50	N/A	N/A
c (z)-axis (m)	4000	N/A	5000	N/A	N/A
Source strike (°)	0	0	90	180	30
Source dip (°)	0	−30	0	30	10
Source heading (°)	0	0	0	180	30
Pressure (MPa)	10	−30	6	30	3
[B] Source parameters (dyke conduit co-parameter test)					
Parameter	Mid-crustal source	Dyke conduit (Rectangular Cuboid)			Step
		Low margin	Default	High margin	
Depth (midpoint) (m)	9500	N/A	2500	N/A	100
X-location	588 500	N/A	588 500	N/A	1000
Y-location	1 848 280	N/A	1 848 280	N/A	1000
a (x)-axis (m)	2000	N/A	500	N/A	100
b (y)-axis (m)	2000	N/A	5000	N/A	100
c (z)-axis (m)	4000	N/A	50	N/A	100
Source strike (°)	0	N/A	0	N/A	30
Source dip (°)	0	N/A	0	N/A	30
Source heading (°)	0	20	N/A	80	10
Pressure (MPa)	10	−30	N/A	30	3

to the sensitivity of the GPS data, and only began to show a significant response at depths of less than 10 km. The closest fit to the GPS data was obtained from a prolate source with a midpoint at 9.5 km pressurised at 10 or 11 MPa (Figure 6); other source parameter results are provided in Table 2 and 3, and used as the mid-crustal source values for steps two and three. These results combined imply that there is a shallower aspect to the magmatic system that is at least partially controlling the line length changes seen on EDJH–EDHE, and also the behaviour of the EDM network as a whole, as this is more sensitive to shallower pressurisation.

3.2 Incorporation of shallow pressure sources

As the deformation signal of a shallow source would likely be confined to the area closest to the vent, the EDM network should theoretically be better placed to detect changes than the GPS sites (Figure 1) [Jackson et al. 1998]. We test this assumption using a shallow magma reservoir or a shallow dyke as an additional deformation source, in tandem with the mid-crustal source.

3.2.1 *Addition of a shallow prolate source*

Firstly, a second, shallow prolate magma reservoir source was added, above the mid-crustal magma reservoir (Table 2). Sensitivity tests of the parameters defining the second prolate source showed that changes to a shallow deformation source of this type produces negligible variation in the modelled surface deformation patterns (Figure 7). The lack of deformation response in both GPS and EDM measurements suggests that the deformation signal from the mid-crustal source overprints the effect of any shallow reservoir-style source (Figure 7). The only parameter variations that induced measurable EDM line length changes were variations to the x and y axes of the shallow source (Figure 7) likely due to the asymmetrical near-field deformation footprint this begins to produce in contrast to the symmetrical deformation field of the 'default' shallow source or the fixed mid-crustal source. The GPS network was also largely unresponsive to changes in the shallow source, although it did result in some minor movement at HERM and LGRD, both situated within 1 km of the vent, and therefore to the source itself (Supplementary Material Figure S4).

From these results, we can infer that when the deformation signal produced by the shallow source is symmetrical it cannot be distinguished from that of the mid-crustal magmatic system. However, asymmetric deformation fields produced by the shallow source, such as when the horizontal axes of the shallow source were non-equal, can have a measurable effect on the EDM monitoring network. The fact that the

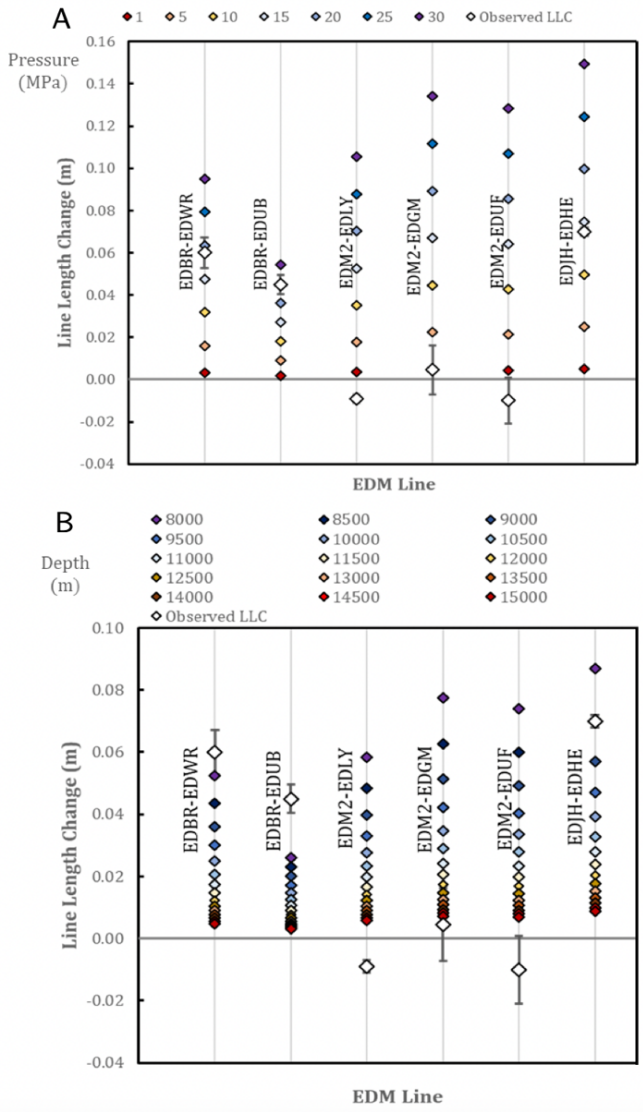

Figure 5: EDM line length change (LLC) sensitivity modelling results from varying the properties of a single, prolate, mid-crustal deformation source, including: [A] source pressure (in MPa), and [B] source depth (in m). Observed data (white diamonds with error bars) are compared against modelled data (coloured diamonds; colours indicated by figure legends). Varying the mid-crustal source alone produced a broadly symmetrical deformation pattern across all EDM lines.

near-vent asymmetric deformation effects were not picked up by the GPS network (HERM and LGRD aside) suggests the deformation produced by a shallow source only affected the area closest to the vent: an area of the volcanic edifice where the EDM network had far greater coverage compared with the GPS network.

3.2.2 *Addition of a shallow dyke source*

Our preliminary sensitivity tests of a shallow dyke conduit source showed that variation in certain source parameters had a significant impact on the fit to the EDM data, far more so than for the GPS data. Additionally, our results show that the asymmetric deformation field produced was measurable above that produced by the mid-crustal magmatic system (Figure 8). The two parameters that produced the most significant changes to misfit values were pressure and change in strike, with misfit values indicating the optimal dyke orientation (or strike) is approximately NW–SE (Figure 8). Therefore, we also undertook a further co-parametric sensitivity test of pressure and orientation in tandem, with a more focused orientation parameter range than the original sensitivity tests (Table 3).

We found that our closest fit to the observed EDM data was achieved by a shallow dyke striking 330° (NNW–SSE) and a pressure of −12 MPa (Figure 9). This dyke orientation is consistent with the tectonic stress field and fault structures surrounding Montserrat [Feuillet et al. 2010] and previous modelling studies into the shallow magmatic system [Mattioli et al. 1998; Costa et al. 2007; Hautmann et al. 2009; Linde et al. 2010]. The deformation field produced by the dyke was small, and only affected a local area of the edifice close to the vent; further away from the vent the dyke-derived deformation field weakened until it was overwritten by the deformation field generated by the mid-crustal magmatic system. The overwhelming majority of the GPS network is situated too far away from the vent to detect the deformation field changes controlled by a shallow dyke conduit source, with the only exception being HERM (and possibly LGRD). However, EDM reflectors are situated close enough to the vent to respond to these shallow source changes.

Negative pressure changes in the dyke source produced line lengthening on all EDM lines (Figure 10), with EDJH–EDHE the most responsive. The line-lengthening deformation was generated due to EDM reflectors close to the vent showing horizontal movement towards the vent in response to negative shallow pressurisation. In contrast, the deformation response of EDM stations further from the vent were determined by the positive pressurisation of the mid-crustal magmatic system, resulting in horizontal movement away from the vent (Figure 11). The opposite movement of both ends of the EDM baselines produces positive EDM line lengthening, as the mid-crustal system pressurises (possibly through magma supply) and the shallow system depressurises, indicating volume contraction, possibly through cooling.

The deformation generated by our best-fit shallow dyke conduit, orientated NNW–SSE and pressurised at −12 MPa is perpendicular to the orientation (or strike) of the dyke (i.e. the deformation is greatest in the direction ENE–WSW). The interaction of the shallow dyke-derived deformation and surface topography means that only a small area of significant deformation was produced that overprinted the more dominant deformation signal of the mid-crustal system (Figure 11). This area encompasses the GPS site HERM (and to a lesser extent, LGRD), and could be a possible explanation for the behaviour of HERM with regards to its deformation pattern differing to the pattern of most other GPS sites.

Overall, the gain of the shallow dyke source in comparison to only the mid-crustal source in terms of the fit to the spatial deformation pattern is marginal (Figure 10, Supplementary Material Figures S7 and S8). While the overall misfit J value is improved, indicating a greater overall bulk fit to the

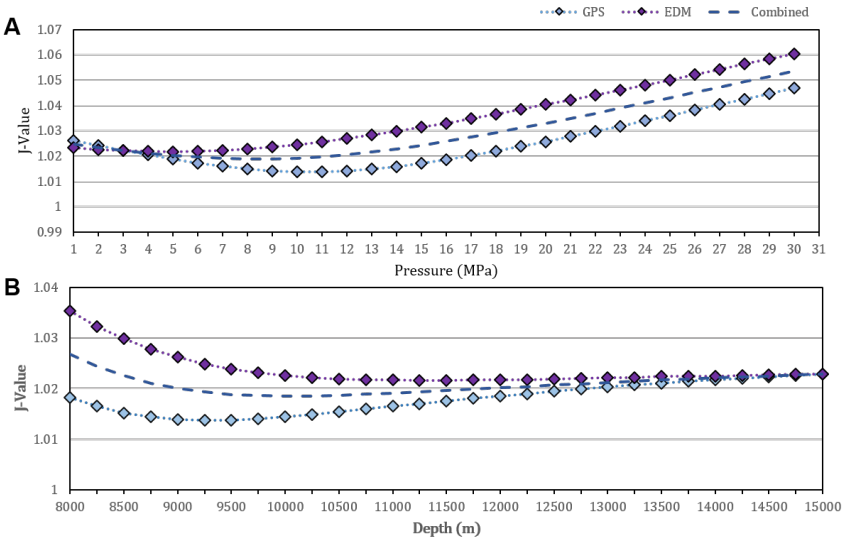

Figure 6: Mid-crustal source sensitivity test results. Misfit (*J*) values with variation of; [A] Pressure and [B] Depth, of a mid-crustal prolate source. The lower the misfit the better the fit of the model to the observed data. The model produces a closer fit to the GPS data than the EDM data, with different optimum pressures (EDM – 4 MPa; GPS – 10 or 11 MPa) and depths (EDM – 11500 m; GPS – 9250 m) for the two datasets when observed independently. Other sensitivity test results are available in Supplementary Material Figure S3. These results are from the initial wider range of values (step 1a).

data, reducing from 1.0216 to 1.0158, only the magnitude of deformation on one EDM line is accurately reproduced (Figure 10). However, the pattern of EDM baseline length changes, in terms of their sign and relative values across the six lines, is improved by the addition of the dyke source, as seen by the comparison of Figure 5 and Figure 10. A more detailed forward exploration of parameters values, or a formal inversion and optimisation against the data, could improve the significance of the model fits, but this was beyond the scope of our study and outside of the main aim of our work, which focussed on characterising the relationships between shallow and mid-crustal deformation sources, and their effects on the surface deformation patterns.

3.3 Prospective new EDM lines

In our tests with two new prospective EDM lines (Figure 12) the modelled results show that on the south-eastern flank DRYG–ENEW1 was relatively unresponsive to pressure changes in the shallow dyke conduit (Figure 13). This is partly due to the shorter starting line length when compared with EDM baselines on the northern flank, as points further away from the vent experienced a greater horizontal deformation effect from the pressurisation of the mid-crustal magmatic system. The relative unresponsiveness of DRYG–ENEW1 is also to some extent a mirror of the reduced line length change seen on EDM2–EDLY/EDGM/EDUF on the north-western flank (when compared with EDJH–EDHE). However, unlike the line length behaviour of EDM2–EDLY/EDGM/EDUF, DRYG–ENEW1 showed increased line lengthening with increasing pressure, the inverse of the modelled behaviour of all other EDM lines in response to the over- or under-pressurisation of a dyke conduit source (Figure 13).

ENEW2–EDWR behaved similarly to other EDM baselines, and produced comparable results to EDBR–EDWR due to sharing a reflector. The reflector EDWR on the south-western flank responded to the pressurisation of the dyke conduit in a similar manner to EDHE on the north-eastern flank (Figure 10 and Figure 13). In contrast, the modelled results for a theoretical EDM baseline ENEW2–EDWR did not provide much insight above what EDBR–EDWR can offer, and does help to illustrate that it is the reflector, not the base station, which defines the line length behaviour in relation to shallow source pressurisation.

In summary, a new EDM line on the south-eastern flank of the volcano (DRYG–ENEW1) would not likely be optimally placed to respond to pressure changes in the shallow magmatic system despite filling a geographical gap in the spatial coverage of the EDM network. In addition, it would be relatively difficult to access due to its position in the island's exclusion zone. While ENEW2–EDWR on the south-western flank is sensitive to shallow source pressurisation, it likely only serves to duplicate the results of EDBR–EDWR, which when combined with the difficulty in accessing the base station site in the exclusion zone means it may not provide good cost-benefit trade-offs.

3.4 Implications

The GPS network on Montserrat is well placed to monitor changes to the mid-crustal magmatic system, however, our results suggest that changes in the shallow system would likely not be detected by the GPS network. The surface displacement footprint of the shallow system is small, partially overprinted by that of the mid-crustal source, and is highly asymmetrical, and as a result displays significant local variation (Figure 11). The GPS site most affected by the surface defor-

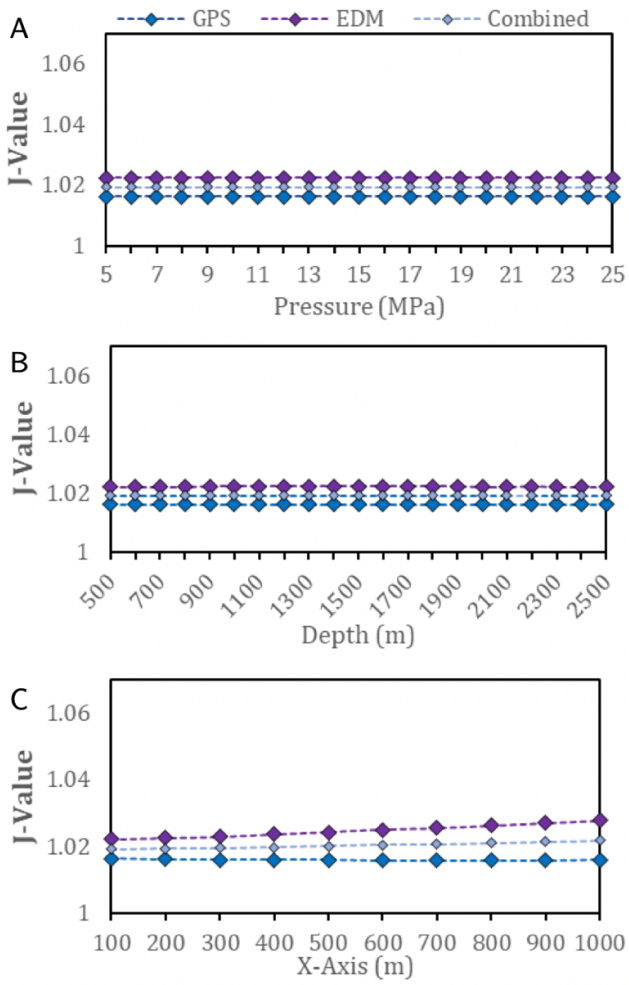

Figure 7: Shallow reservoir sensitivity test results. Changes to misfit (*J*) value with: [A] Pressure variation of a shallow reservoir style source and a fixed mid-crustal source; [B] Depth variation of a shallow reservoir source and a fixed mid-crustal source; and [C] X-Axis variation of the shallow source and a fixed mid-crustal source. There is no change to the fit of the model with variation of the shallow source pressure or depth, but there is some minor impact on fit to the EDM data alone when the horizontal axes of the shallow source are changed. Negative pressure values were tested alongside positive values, and produced similar results. Other sensitivity test results are available in Supplementary Material Figure S5.

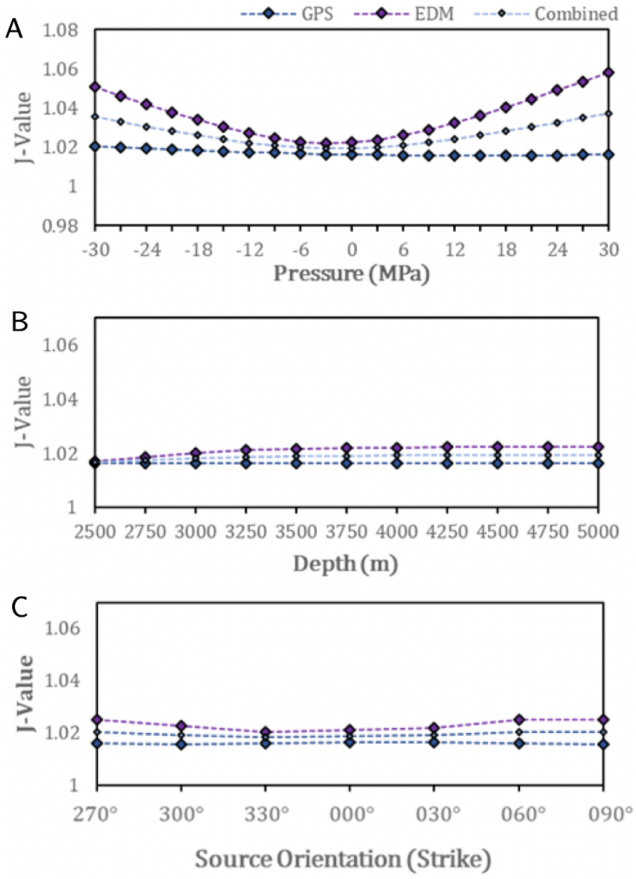

Figure 8: Shallow dyke conduit sensitivity test results. Changes to misfit (*J*) value for: [A] Pressure in a shallow dyke conduit; [B] Depth of shallow dyke conduit; and [C] Strike of shallow dyke conduit (measured in both degrees from East and Strike). Pressure was the parameter that the results were most sensitive to, followed by source strike. Both EDM and GPS networks were largely unresponsive to depth changes, except for EDM at depths shallower than 3000 m, with the closest fit obtained at 2500 m. Other parameter variations largely failed to produce meaningful deformation responses, although other parameters that changed the symmetry of the deformation field produced by the shallow source such as source heading, x-location, and y-location, did have a minor effect. The GPS response to all parameter variation was negligible, with pressure being the exception, and this was minor when compared to the response to pressure recorded by EDM. Other sensitivity test results are available in Supplementary Material Figure S6.

mation footprint of the shallow dyke source is HERM. The placement of HERM and EDHE within the displacement footprint (Figure 11) of our modelled shallow dyke source potentially explains the unusual displacement observed at the site relative to the rest of the GPS network, as the east–west, north–south, and vertical displacement components of the shallow dyke source have different relative amplitudes. The co-location of HERM and EDHE is in an area which our model predicts will respond strongly to the north–south displacement component of the displacement field of the shallow dyke, weakly to the east–west displacement component, and insignificantly to the vertical displacement component. This has the effect of north–south deformation signals at HERM and EDHE being controlled primarily by the shallow dyke conduit, with southward movement likely to be detected as the dyke contracts. However, the east-west and vertical displacement of the site would be controlled by the behaviour of the mid-crustal source, causing the uplift and eastward component of the migration of the site observed between 2010 and 2019. There could also be an element of edifice decoupling causing the ridge upon which HERM and EDHE are situated to deform in a different way to the rest of the edifice [McPherson 2013; Odbert et al. 2014].

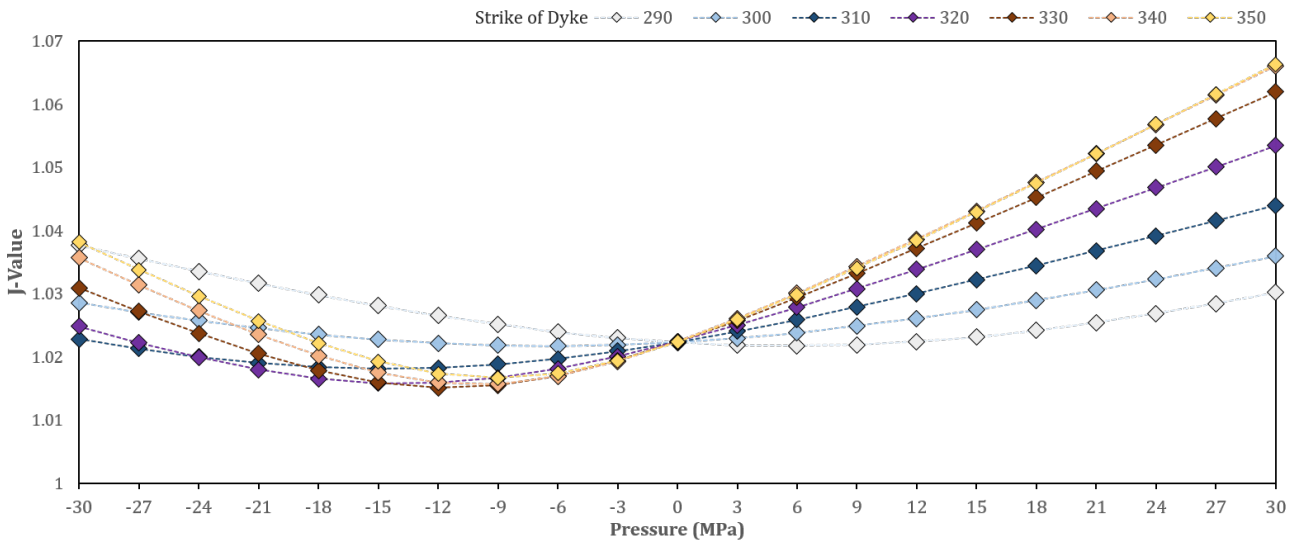

Figure 9: Co-parameter variation misfit results, with the misfit (*J*) values from variation of pressure and orientation of a shallow dyke source above a fixed mid-crustal source. The closest fits (lowest *J*-values) were obtained by negative pressures in the shallow system. Our best overall fit was in a dyke striking 330° (NNW–SSE) and a pressure of –12 MPa.

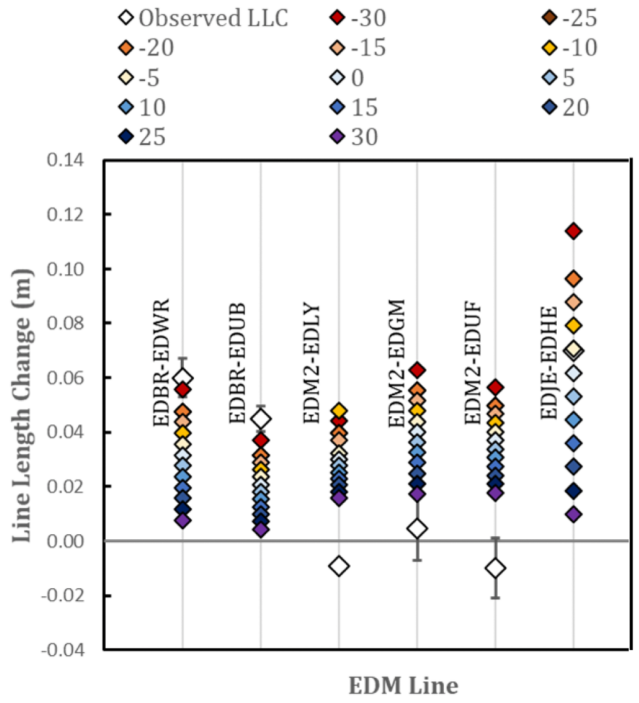

Figure 10: Co-parameter variation EDM results with line responses to pressure variation of a shallow dyke source (placed above a mid-crustal magmatic system pressurised at 10 MPa) striking 330°. Different coloured symbols represent results of different source pressurisation (MPa). The increased sensitivity of the north-eastern flank (specifically reflector site EDHE) to pressure changes in a dyke source is seen here in the increased range of line length change values to the same pressure variation, with negative pressurisation generating greater line length extension.

EDM reflectors are generally situated much closer to the vent than GPS stations on Montserrat, and as a result are better placed to respond to changes in the shallow system. Interpretation of EDM line length changes should consider that each end of the line is responding to different parts of the magmatic system. EDM base stations away from the vent respond to changes in the mid-crustal magmatic system similar to the GPS network, whereas the EDM reflectors close to the vent respond predominantly to changes in the shallow system. However, the exact location of the EDM reflectors is vital due to the substantial local variation in surface deformation behaviour close to the vent produced by topographical effects and the likely asymmetry of the deformation field associated with the shallow dyke. EDM line EDJH–EDHE is best placed to detect changes in the shallow system at the SHV, as the EDM reflector EDHE is well within the deformation footprint of the shallow dyke conduit (Figure 11), as is the GPS station HERM. The EDM lines EDBR–EDUB/EDWR are also reasonably well placed to detect changes in the shallow dyke conduit; similarly, this may also explain why GPS sites on the edge of the deformation footprint from the shallow dyke source (FRGR, NWHT, and SPRI) have horizontal displacement velocities that do not conform to the wider symmetrically radial GPS deformation pattern recorded by the wider GPS network.

From our results for the best fits to negative pressurisation in the shallow system, and the behaviour of HERM and EDJH–EDHE, we can interpret that the current shallow system behaviour is likely one of cooling and contraction. The results from the GPS network suggest the mid-crustal magmatic system is still being pressurised at about 10 MPa between 2010 and 2019, but it is not causing any reactivation in the shallow system at present. The overpressure of the mid-crustal magmatic system would likely drop during an eruptive phase as magma moves up through the system, pos-

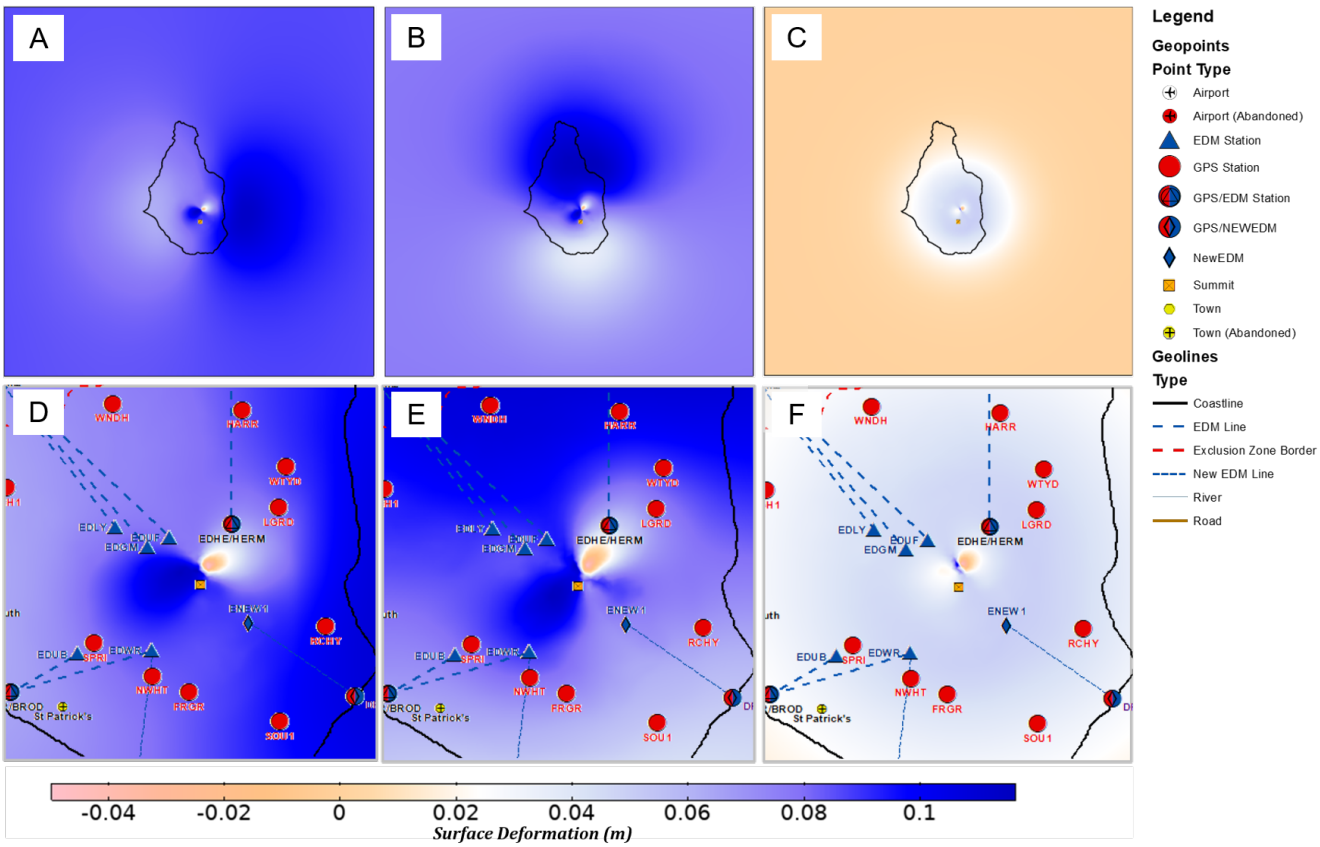

Figure 11: Surface deformation maps, cropped from the full model domain. Plots of modelled surface deformation, with a mid-crustal source pressurised at 10 MPa, and a shallow dyke striking 330° clockwise from North and pressurised at –12 MPa. The top row shows the full view of Montserrat with deformation patterns predominantly caused by the mid-crustal magmatic system: [A] East–west deformation; [B] North–south deformation; and [C] Vertical deformation. The bottom row shows a zoomed-in field-of-view near the vent, better highlighting the deformation footprint produced by the dyke: [D] East–west deformation; [E] North–south deformation; and [F] Vertical deformation. All maps are orientated with north at the top.

itively pressurising the shallow dyke conduit. The likely pattern of pressurisation in the immediate build-up to eruptive activity would flip the pattern of behaviour in both EDM and GPS observed in the current pause state. This would present as GPS sites distal to the vent showing horizontal deformation towards the vent, HERM showing horizontal deformation away from the vent (north-eastward movement), EDJH–EDHE, EDBR–EDWR, and EDBR–EDUB showing significant shortening, and EDM2–EDGM and EDM2–EDUF relatively unresponsive. For future monitoring of the island, this could mean that over-pressurisation of the shallow conduit would present as north-eastward horizontal deformation of HERM, and line length shortening of EDJH–EDHE, as these would likely be the best indicators of shallow system behaviour.

For application to other volcanoes, EDM could provide a cheaper and safer way to effectively monitor the shallow magmatic system than GPS, as reflectors can be set up quickly, measurements taken from a safe distance, and equipment can be replaced at a much cheaper cost if destroyed. Covering multiple flanks to find possible dyke conduit orientations and monitor shallow system behaviour is important, as half the area close to the vent may still be relatively unresponsive to a dyke source pressurisation. Installing multiple GPS monitoring sites close to the vent may be impossible for many volcano observatories, either due to a lack of appropriate sites, or to financial or safety constraints, leading to limited and incomplete coverage of shallow system processes. For installing new sites, priority should be given to the flanks perpendicular to the likely dyke orientation as determined by the regional stress field [Anderson 1906], as these will be the most responsive to pressurisation of the dyke. Tiltmeters have also been used to monitor volcanic edifice deformation [e.g. Costa et al. 2007; Hautmann et al. 2009; Johnson et al. 2019], but compared to EDM they are more expensive and resource-intensive to install and maintain.

3.5 Limitations

The model uses a heterogeneous elastic domain, which does not consider the effects of viscoelasticity [Del Negro et al. 2009; Hickey et al. 2016; Head et al. 2019; Sigmundsson et al. 2020] on the rheological behaviour. A temperature dependent viscoelastic medium would likely result in lower overpressure requirements for the mid-crustal source due to thermal weakening of the Young's modulus and enhanced deformation from the viscous component [Head et al. 2021]. The pressure value of the shallow dyke source is unlikely to be strongly affected,

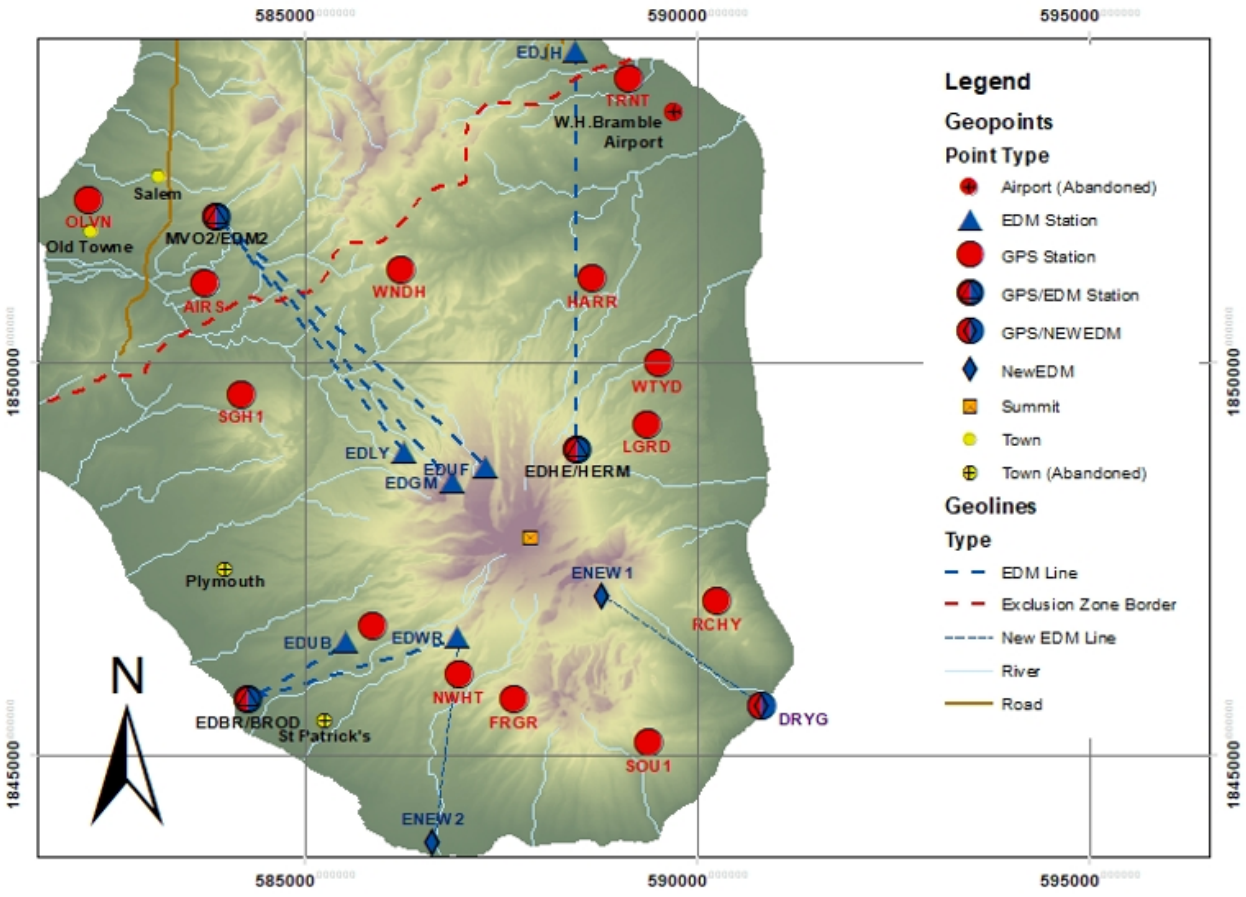

Figure 12: EDM monitoring network map which this study draws data from. Two additional theoretical EDM line locations are shown which were experimented with in this study to infer deformation behaviour on the southern and south-eastern flanks, which currently lack EDM monitoring capability.

as the colder shallow crust should behave in an elastic manner [Ranalli 1995]. The recorded deformation at SHV is time-dependent, and this may be representative of time-variable source processes in an elastic rheology, or arise due to time-dependent (e.g. viscoelastic) crustal rheology, or a combination of the two. Viscoelastic processes have been ruled out of playing a dominant role in the recorded deformation at SHV [Hickey et al. 2022], and so our choice of an elastic rheology is sufficient for a first-order exploration of the problem we address.

The shape of the dyke is a simplified rectangular cuboid, with a thickness of 50 m, to reduce mesh density and computing (RAM) requirements. Previous investigations into the dyke found the width to be as narrow as 2 m [Costa et al. 2007; Hautmann et al. 2009]. To quantify the effect of the increased dyke thickness imposed upon our study we ran a comparison of a 2 m wide-dyke and a 50 m wide dyke with equal pressure and geometry in a 2D elastic medium. There is no significant difference to the surface deformation response caused by the increase in dyke thickness (Supplementary Material Figure S2), and therefore this limitation does not have a significant impact on our deformation results. However, future work should endeavour to use a 2 m wide dyke as suggested by previous work. This improvement may allow for an investigation into possible volume contraction rates to compare against thermal models in order to potentially distinguish between future magma withdrawal and magma cooling and contraction as the physical mechanisms driving the underpressurisation of the dyke source. Additionally, through our forward model approach we manually tested a range of model parameters (e.g. source pressures, sizes, and depths) and consequently our 'best fits' are only certain across the discrete values used; alternative solutions with improved fits to the observed data may exist that we did not explicitly test here.

The hydrothermal system at the SHV is extensive, being at least 2 km in diameter and extending approximately 800 m below the vent [Boudon et al. 1998]. Perturbation of the hydrothermal system produces measurable deformation, and is responsible for much of the noise in the observed EDM data (Supplementary Material Figure S1). The exact extent of hydrothermally-derived deformation on the overall deformation patterns observed at the SHV is still largely unknown.

4 Conclusions

1. The pattern of EDM line length changes recorded at SHV between 2010 and 2019 cannot be solely explained by

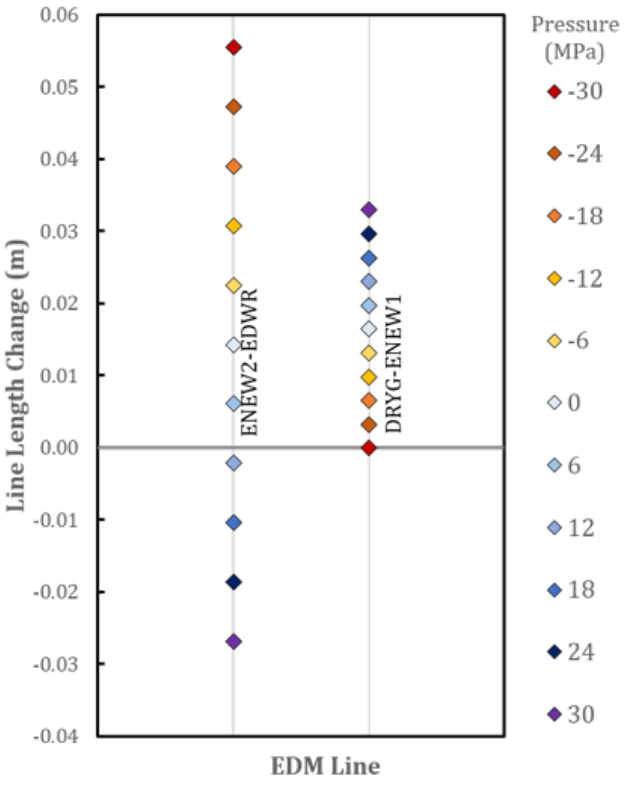

Figure 13: EDM line modelling results for two potential baselines showing predicted line length changes due to pressure variation in a shallow dyke source with a strike of 330° (NNW–SSE).

the effects of a mid-crustal deformation source, or with the addition of a shallow prolate magma reservoir.

2. The modelled spatial deformation field is sensitive to variations of a dyke conduit shallow source. Pressure and orientation parameters have the greatest influence. However, the spatial extent of the deformation field produced by a shallow source only affects a small area of the edifice close to the vent, including the EDM reflectors and HERM and LGRD GPS stations only; deformation at distal locations is dictated by the mid-crustal magmatic system.

3. Varying the orientation and pressure of a shallow dyke source simultaneously found that our closest fit to the observed EDM data was for a shallow dyke striking 330° (NNW–SSE) with a pressure of −12 MPa. Negative pressure values consistently produced closer fits to the observed data than positive pressure values. This could be explained by cooling and contraction, while the mid-crustal system is still being pressurised (to ~10 MPa), possibly due to magma supply from depth.

4. At a strike of 330°, negative pressurisation of the dyke caused a small area on the north-eastern flank of the volcano to deform horizontally to the southwest, including the GPS site HERM and the EDM reflector EDHE. We conclude that the behaviour of HERM is potentially due to HERM responding to a combination of pressure changes in the shallow dyke conduit and mid-crustal system, while the rest of the GPS network responded to pressure changes in the mid-crustal system only.

5. For future monitoring purposes, the behaviour of HERM and the EDM network (especially EDJH–EDHE), are likely indicative of pressure changes in the shallow system. Eastward and northward migration of HERM, or line length shortening of EDJH–EDHE, and EDBR–EDUB/EDWR, could indicate pressurisation of the shallow magmatic system.

6. EDM can provide a safer, quicker, and cheaper way of effectively monitoring shallow system processes than GPS, as coverage of multiple flanks close (within 1 km) to the vent is vital for understanding the behaviour of dyke conduit-shaped shallow magmatic system processes given they produce highly asymmetrical deformation fields. When choosing monitoring sites to target the shallow system, preference should be given to those on lines perpendicular to the expected dyke orientation as determined by the regional and local stress fields, as these areas are more sensitive to deformation changes in the shallow magmatic system.

Author Contributions

A.J, J.H, and K.P derived the lines of investigation. Primary data collection and processing was undertaken by K.P. and R.S. Data post-processing, modelling, and analysis of results was done by A.J. Manuscript drafting was undertaken by A.J, with all authors contributing to the final version.

Acknowledgements

We would like to thank the Montserrat Volcano Observatory for the continual monitoring networks maintenance and/or development and data collection and processing that made this study possible. We also thank the editors and anonymous reviewers whose feedback helped to improve the manuscript.

Data Availability

The GPS and EDM data that support the findings of this study are available from the Montserrat Volcano Observatory. Restrictions apply to the availability of these data, which were used under license (MVO Data licence DL-2019-Johnson), and so are not publicly available.

Copyright Notice

References

Anderson, E. M. (1906). "The Dynamics of Faulting". *The Journal of Geology* 14(3), pages 254–257. DOI: 10.1086/621305.

Biggs, J. and M. E. Pritchard (2017). "Global Volcano Monitoring: What Does It Mean When Volcanoes Deform?" *Elements* 13(1), pages 17–22. ISSN: 1811-5217. DOI: 10.2113/gselements.13.1.17.

Bonaccorso, A., G. Currenti, and C. Del Negro (2013). "Interaction of volcano-tectonic fault with magma storage, intrusion and flank instability: A thirty years study at Mt. Etna volcano". *Journal of Volcanology and Geothermal Research* 251, pages 127–136. ISSN: 0377-0273. DOI: 10.1016/j.jvolgeores.2012.06.002.

Boudon, G., B. Villemant, J.-C. Komorowski, P. Ildefonse, and M. P. Semet (1998). "The hydrothermal system at Soufriere Hills Volcano, Montserrat (West Indies): Characterization and role in the on-going eruption". *Geophysical Research Letters* 25(19), pages 3693–3696. ISSN: 0094-8276. DOI: 10.1029/98gl00985.

Cabaniss, H. E., P. M. Gregg, S. L. Nooner, and W. W. Chadwick (2020). "Triggering of eruptions at Axial Seamount, Juan de Fuca Ridge". *Scientific Reports* 10(1). ISSN: 2045-2322. DOI: 10.1038/s41598-020-67043-0.

Christopher, T. E., M. C. S. Humphreys, J. Barclay, K. Genareau, S. M. H. D. Angelis, M. Plail, and A. Donovan (2014). "Chapter 17 Petrological and geochemical variation during the Soufrière Hills eruption, 1995 to 2010". *Geological Society, London, Memoirs* 39(1), pages 317–342. DOI: 10.1144/m39.17.

Costa, A., O. Melnik, R. S. J. Sparks, and B. Voight (2007). "Control of magma flow in dykes on cyclic lava dome extrusion". *Geophysical Research Letters* 34(2). DOI: 10.1029/2006gl027466.

Currenti, G., C. Del Negro, and G. Ganci (2007). "Modelling of ground deformation and gravity fields using finite element method: an application to Etna volcano". *Geophysical Journal International* 169(2), pages 775–786. ISSN: 1365-246X. DOI: 10.1111/j.1365-246x.2007.03380.x.

Del Negro, C., G. Currenti, and D. Scandura (2009). "Temperature-dependent viscoelastic modeling of ground deformation: Application to Etna volcano during the 1993–1997 inflation period". *Physics of the Earth and Planetary Interiors* 172(3–4), pages 299–309. ISSN: 0031-9201. DOI: 10.1016/j.pepi.2008.10.019.

Dragoni, M. and C. Magnanensi (1989). "Displacement and stress produced by a pressurized, spherical magma chamber, surrounded by a viscoelastic shell". *Physics of the Earth and Planetary Interiors* 56(3-4), pages 316–328. DOI: 10.1016/0031-9201(89)90166-0.

Elsworth, D., G. Mattioli, J. Taron, B. Voight, and R. Herd (2008). "Implications of Magma Transfer Between Multiple Reservoirs on Eruption Cycling". *Science* 322(5899), pages 246–248. ISSN: 1095-9203. DOI: 10.1126/science.1161297.

Feuillet, N., F. Leclerc, P. Tapponnier, F. Beauducel, G. Boudon, A. Le Friant, C. Deplus, J.-F. Lebrun, A. Nercessian, J.-M. Saurel, and V. Clément (2010). "Active faulting induced by slip partitioning in Montserrat and link with volcanic activity: New insights from the 2009 GWADASEIS marine cruise data". *Geophysical Research Letters* 37(19). ISSN: 0094-8276. DOI: 10.1029/2010gl042556.

Fialko, Y., Y. Khazan, and M. Simons (2001). "Deformation due to a pressurized horizontal circular crack in an elastic half-space, with applications to volcano geodesy". *Geophysical Journal International* 146(1), pages 181–190. ISSN: 1365-246X. DOI: 10.1046/j.1365-246x.2001.00452.x.

Fournier, N. and L. Chardot (2012). "Understanding volcano hydrothermal unrest from geodetic observations: Insights from numerical modeling and application to White Island volcano, New Zealand". *Journal of Geophysical Research: Solid Earth* 117(B11). ISSN: 0148-0227. DOI: 10.1029/2012jb009469.

Geirsson, H., P. LaFemina, T. Árnadóttir, E. Sturkell, F. Sigmundsson, M. Travis, P. Schmidt, B. Lund, S. Hreinsdóttir, and R. Bennett (2012). "Volcano deformation at active plate boundaries: Deep magma accumulation at Hekla volcano and plate boundary deformation in south Iceland". *Journal of Geophysical Research: Solid Earth* 117(B11). ISSN: 0148-0227. DOI: 10.1029/2012jb009400.

Gottsmann, J., M. Flynn, and J. Hickey (2020). "The Transcrustal Magma Reservoir Beneath Soufrière Hills Volcano, Montserrat: Insights From 3-D Geodetic Inversions". *Geophysical Research Letters* 47(20). ISSN: 1944-8007. DOI: 10.1029/2020gl089239.

Gottsmann, J., J.-C. Komorowski, and J. Barclay (2017). "Volcanic Unrest and Pre-eruptive Processes: A Hazard and Risk Perspective". *Advances in Volcanology*. Edited by J. Gottsmann, J. Neuberg, and B. Scheu. Springer International Publishing, pages 1–21. DOI: 10.1007/11157_2017_19.

Gottsmann, J. and H. M. Odbert (2014). "The effects of thermomechanical heterogeneities in island arc crust on time-dependent preeruptive stresses and the failure of an andesitic reservoir". *Journal of Geophysical Research: Solid Earth* 119(6), pages 4626–4639. ISSN: 2169-9313. DOI: 10.1002/2014jb011079.

Hautmann, S., J. Gottsmann, R. S. J. Sparks, A. Costa, O. Melnik, and B. Voight (2009). "Modelling ground deformation caused by oscillating overpressure in a dyke conduit at Soufrière Hills Volcano, Montserrat". *Tectonophysics* 471(1–2), pages 87–95. ISSN: 0040-1951. DOI: 10.1016/j.tecto.2008.10.021.

Hautmann, S., D. Hidayat, N. Fournier, A. T. Linde, I. S. Sacks, and C. P. Williams (2013). "Pressure changes in the magmatic system during the December 2008/January 2009 extrusion event at Soufrière Hills Volcano, Montserrat (W.I.), derived from strain data analysis". *Journal of Volcanology and Geothermal Research* 250, pages 34–41. ISSN: 0377-0273. DOI: 10.1016/j.jvolgeores.2012.10.006.

Head, M., J. Hickey, J. Gottsmann, and N. Fournier (2019). "The Influence of Viscoelastic Crustal Rheologies on Volcanic Ground Deformation: Insights From Models of Pressure and Volume Change". *Journal of Geophysical Research: Solid Earth* 124(8), pages 8127–8146. ISSN: 2169-9356. DOI: 10.1029/2019jb017832.

– (2021). "Exploring the Impact of Thermally Controlled Crustal Viscosity on Volcanic Ground Deformation". *Journal of Geophysical Research: Solid Earth* 126(8). DOI: 10.1029/2020jb020724.

Herring, T. A., R. W. King, M. A. Floyd, and S. C. McClusky (2018). *Introduction to GAMIT/GLOBK*. URL: http://geoweb.mit.edu/gg/Intro_GG.pdf (visited on 08/11/2023). Massachusetts Institute of Technology.

Hickey, J. (2015). "Constraining volcanic unrest with integrated geodetic modelling". PhD thesis. University of Bristol.

Hickey, J. and J. Gottsmann (2014). "Benchmarking and developing numerical Finite Element models of volcanic deformation". *Journal of Volcanology and Geothermal Research* 280, pages 126–130. DOI: 10.1016/j.jvolgeores.2014.05.011.

Hickey, J., J. Gottsmann, P. Mothes, H. M. Odbert, I. Prutkin, and P. Vajda (2017). "The Ups and Downs of Volcanic Unrest: Insights from Integrated Geodesy and Numerical Modelling". *Volcanic Unrest*, pages 203–219. ISSN: 2364-3285. DOI: 10.1007/11157_2017_13.

Hickey, J., J. Gottsmann, H. Nakamichi, and M. Iguchi (2016). "Thermomechanical controls on magma supply and volcanic deformation: application to Aira caldera, Japan". *Scientific Reports* 6(1). ISSN: 2045-2322. DOI: 10.1038/srep32691.

Hickey, J., R. Lloyd, J. Biggs, D. Arnold, P. Mothes, and C. Muller (2020). "Rapid localized flank inflation and implications for potential slope instability at Tungurahua volcano, Ecuador". *Earth and Planetary Science Letters* 534, page 116104. ISSN: 0012-821X. DOI: 10.1016/j.epsl.2020.116104.

Hickey, J., K. Pascal, M. Head, J. Gottsmann, N. Fournier, S. Hreinsdottir, and R. Syers (2022). "Magma pressurization sustains ongoing eruptive episode at dome-building Soufrière Hills volcano, Montserrat". *Geology* 50(11), pages 1261–1265. ISSN: 1943-2682. DOI: 10.1130/g50239.1.

Jackson, P., J. B. Shepherd, R. E. A. Robertson, and G. Skerritt (1998). "Ground deformation studies at Soufriere Hills Volcano, Montserrat I: Electronic distance meter studies". *Geophysical Research Letters* 25(18), pages 3409–3412. DOI: 10.1029/98gl01656.

Johnson, J. H., M. P. Poland, K. R. Anderson, and J. Biggs (2019). "A Cautionary Tale of Topography and Tilt from Kīlauea Caldera". *Geophysical Research Letters* 46(8), pages 4221–4229. ISSN: 1944-8007. DOI: 10.1029/2018gl081757.

Linde, A. T., S. Sacks, D. Hidayat, B. Voight, A. Clarke, D. Elsworth, G. Mattioli, P. Malin, E. Shalev, S. Sparks, and C. Widiwijayanti (2010). "Vulcanian explosion at Soufrière Hills Volcano, Montserrat on March 2004 as revealed by strain data". *Geophysical Research Letters* 37(19). ISSN: 0094-8276. DOI: 10.1029/2009gl041988.

Loughlin, S., B. Baptie, T. Christopher, G. .Ryan, R. Luckett, V. Hards, L. Jones, N. Fournier, V. Bass, T. Syers, L. Ruzié, M. Higgins, P. Williams, and D. Williams (2006). "Report to the Scientific Advisory Committee". *Montserrat Open File Report* 06-07.

Masterlark, T. (2007). "Magma intrusion and deformation predictions: Sensitivities to the Mogi assumptions". *Journal of Geophysical Research* 112(B6). ISSN: 0148-0227. DOI: 10.1029/2006jb004860.

Mattioli, G. S., T. H. Dixon, F. Farina, E. S. Howell, P. E. Jansma, and A. L. Smith (1998). "GPS measurement of surface deformation around Soufriere Hills Volcano, Montserrat from October 1995 to July 1996". *Geophysical Research Letters* 25(18), pages 3417–3420. ISSN: 0094-8276. DOI: 10.1029/98gl00931.

Mattioli, G. S., R. A. Herd, M. H. Strutt, G. Ryan, C. Widiwijayanti, and B. Voight (2010). "Long term surface deformation of Soufrière Hills Volcano, Montserrat from GPS geodesy: Inferences from simple elastic inverse models". *Geophysical Research Letters* 37(19). ISSN: 0094-8276. DOI: 10.1029/2009gl042268.

McPherson, E. E. (2013). "A Model Of Short Term Surface Deformation Of Soufriere Hills Volcano, Montserrat Constrained By GPS Geodesy". Master's thesis. University of Texas at Arlington.

Melnik, O. and R. S. J. Sparks (2002). "Modelling of conduit flow dynamics during explosive activity at Soufrière Hills Volcano, Montserrat". *Geological Society, London, Memoirs* 21(1), pages 307–317. DOI: 10.1144/gsl.mem.2002.21.01.14.

Mogi, K. (1958). "Relations between the eruptions of various volcanoes and the deformations of the ground surfaces around them". *Bulletin of the Earthquake Research Institute* 36, pages 99–134.

Neuberg, J., B. Taisne, M. Burton, G. Ryan, E. Calder, N. Fournier, and A. Collinson (2022). "A review of tectonic, elastic and visco-elastic models exploring the deformation patterns throughout the eruption of Soufrière Hills volcano on Montserrat, West Indies". *Journal of Volcanology and Geothermal Research* 425, page 107518. ISSN: 0377-0273. DOI: 10.1016/j.jvolgeores.2022.107518.

Odbert, H. M., G. A. Ryan, G. S. Mattioli, S. Hautmann, J. Gottsmann, N. Fournier, and R. A. Herd (2014). "Chapter 11 Volcano geodesy at the Soufrière Hills Volcano, Montserrat: a review". *Geological Society, London, Memoirs* 39(1), pages 195–217. ISSN: 2041-4722. DOI: 10.1144/m39.11.

Odbert, H. M., B. Taisne, and J. Gottsmann (2015). "Deposit loading and its effect on co-eruptive volcano deformation". *Earth and Planetary Science Letters* 413, pages 186–196. ISSN: 0012-821X. DOI: 10.1016/j.epsl.2015.01.005.

Parker, A. L., J. Biggs, and Z. Lu (2014). "Investigating long-term subsidence at Medicine Lake Volcano, CA, using multitemporal InSAR". *Geophysical Journal International* 199(2), pages 844–859. ISSN: 0956-540X. DOI: 10.1093/gji/ggu304.

Paulatto, M., C. Annen, T. J. Henstock, E. Kiddle, T. A. Minshull, R. S. J. Sparks, and B. Voight (2012). "Magma chamber properties from integrated seismic tomography and thermal modeling at Montserrat". *Geochemistry, Geophysics, Geosystems* 13(1). ISSN: 1525-2027. DOI: 10.1029/2011gc003892.

Phillipson, G., R. Sobradelo, and J. Gottsmann (2013). "Global volcanic unrest in the 21st century: An analysis of the first decade". *Journal of Volcanology and Geothermal Research* 264, pages 183–196. ISSN: 0377-0273. DOI: 10.1016/j.jvolgeores.2013.08.004.

Ranalli, G. (1995). *Rheology of the Earth*. 2nd edition. Springer Science & Business Media. ISBN: 0-412-54670-1.

Sigmundsson, F., V. Pinel, R. Grapenthin, A. Hooper, S. A. Halldórsson, P. Einarsson, B. G. Ófeigsson, E. R. Heimisson, K. Jónsdóttir, M. T. Gudmundsson, K. Vogfjörd, M. Parks, S. Li, V. Drouin, H. Geirsson, S. Dumont, H. M. Fridriksdottir, G. B. Gudmundsson, T. J. Wright, and T. Yamasaki (2020). "Unexpected large eruptions from buoyant magma bodies within viscoelastic crust". *Nature Communications* 11(1). ISSN: 2041-1723. DOI: 10.1038/s41467-020-16054-6.

Spaans, K. and A. Hooper (2016). "InSAR processing for volcano monitoring and other near-real time applications". *Journal of Geophysical Research: Solid Earth* 121(4), pages 2947–2960. ISSN: 2169-9313. DOI: 10.1002/2015jb012752.

Sparks, R. S. J. and S. R. Young (2002). "The eruption of Soufrière Hills Volcano, Montserrat (1995-1999): overview of scientific results". *Geological Society, London, Memoirs* 21(1), pages 45–69. ISSN: 2041-4722. DOI: 10.1144/gsl.mem.2002.021.01.03.

Sparks, R. S. J. and K. V. Cashman (2017). "Dynamic Magma Systems: Implications for Forecasting Volcanic Activity". *Elements* 13(1), pages 35–40. ISSN: 1811-5217. DOI: 10.2113/gselements.13.1.35.

Stinton, A. (2015). "A new Digital Elevation Model of the Soufrière Hills Volcano, Montserrat". *Montserrat Open File Report* 15-01, pages 1–18.

Taylor, N. C., J. H. Johnson, and R. A. Herd (2021). "Making the most of the Mogi model: Size matters". *Journal of Volcanology and Geothermal Research* 419, page 107380. DOI: 10.1016/j.jvolgeores.2021.107380.

Voight, B., A. T. Linde, I. S. Sacks, G. S. Mattioli, R. S. J. Sparks, D. Elsworth, D. Hidayat, P. E. Malin, E. Shalev, C. Widiwijayanti, S. R. Young, V. Bass, A. Clarke, P. Dunkley, W. Johnston, N. McWhorter, J. Neuberg, and P. Williams (2006). "Unprecedented pressure increase in deep magma reservoir triggered by lava-dome collapse". *Geophysical Research Letters* 33(3). ISSN: 0094-8276. DOI: 10.1029/2005gl024870.

Voight, B., D. Hidayat, S. Sacks, A. Linde, L. Chardot, A. Clarke, D. Elsworth, R. Foroozan, P. Malin, G. Mattioli, N. McWhorter, E. Shalev, R. S. J. Sparks, C. Widiwijayanti, and S. R. Young (2010). "Unique strainmeter observations of Vulcanian explosions, Soufrière Hills Volcano, Montserrat, July 2003". *Geophysical Research Letters* 37(19). DOI: 10.1029/2010gl042551.

Wadge, G., G. Mattioli, and R. Herd (2006). "Ground deformation at Soufrière Hills Volcano, Montserrat during 1998–2000 measured by radar interferometry and GPS". *Journal of Volcanology and Geothermal Research* 152(1–2), pages 157–173. ISSN: 0377-0273. DOI: 10.1016/j.jvolgeores.2005.11.007.

Wadge, G., B. Voight, R. S. J. Sparks, P. D. Cole, S. C. Loughlin, and R. E. A. Robertson (2014). "Chapter 1 An overview of the eruption of Soufrière Hills Volcano, Montserrat from 2000 to 2010". *Geological Society, London, Memoirs* 39(1), pages 1–40. DOI: 10.1144/m39.1.

Widiwijayanti, C. (2005). "Geodetic constraints on the shallow magma system at Soufrière Hills Volcano, Montserrat". *Geophysical Research Letters* 32(11). DOI: 10.1029/2005gl022846.

Yang, X.-M., P. M. Davis, and J. H. Dieterich (1988). "Deformation from inflation of a dipping finite prolate spheroid in an elastic half-space as a model for volcanic stressing". *Journal of Geophysical Research: Solid Earth* 93(B5), pages 4249–4257. ISSN: 0148-0227. DOI: 10.1029/jb093ib05p04249.

Young, N. K. and J. Gottsmann (2015). "Shallow crustal mechanics from volumetric strain data: Insights from Soufrière Hills Volcano, Montserrat". *Journal of Geophysical Research: Solid Earth* 120(3), pages 1559–1571. ISSN: 2169-9313. DOI: 10.1002/2014jb011551.